Draft version October 22, 2026
Typeset using LaTeX **twocolumn** style in AASTeX7.0.1

arXiv:2610.28735v1 [astro-ph.GA] 20 Oct 2026

Discovery of a Broad-Line Active Galactic Nucleus at $z = 9.98$

Xingyao Cai [1], Akio K. Inoue [1,2], Masafusa Onoue [3,4], Suzuka Arai [1], Yoshinobu Fudamoto [5], Rohan P. Naidu [6], Pascal A. Oesch [7,8], Jenny E. Greene [9], Ivo Labbe [10], Jorryt Matthee [11], Anna de Graaff [12], Yuma Sugahara [13], Ken Mawatari [14], Pratika Dayal [15,16,17] and Xi Kang [18,19]

[1] *Department of Pure and Applied Physics, Graduate School of Advanced Science and Engineering, Faculty of Science and Engineering, Waseda University, Shinjuku, Tokyo 169-8555, Japan*
[2] *Waseda Research Institute for Science and Engineering, Faculty of Science and Engineering, Waseda University, Shinjuku, Tokyo 169-8555, Japan*
[3] *Waseda Institute for Advanced Study (WIAS), Waseda University, 1-21-1, Nishi-Waseda, Shinjuku, Tokyo 169-0051, Japan*
[4] *Kavli Institute for the Physics and Mathematics of the Universe (WPI), The University of Tokyo Institutes for Advanced Study, The University of Tokyo, Kashiwa, Chiba 277-8583, Japan*
[5] *Center for Frontier Science, Chiba University, 1-33 Yayoi-cho, Inage-ku, Chiba 263-8522, Japan*
[6] *Institute for Astronomy, University of Hawai'i at Mānoa, 2680 Woodlawn Drive, Honolulu, HI 96822, USA*
[7] *Department of Astronomy, University of Geneva, Chemin Pegasi 51, 1290 Versoix, Switzerland*
[8] *Cosmic DAWN Center, Niels Bohr Institute, University of Copenhagen, Jagtvej 128, København N, DK-2200, Denmark*
[9] *Department of Astrophysical Sciences, Princeton University, 4 Ivy Lane, Princeton, NJ 08544, USA*
[10] *Centre for Astrophysics and Supercomputing, Swinburne University of Technology, Melbourne, VIC 3122, Australia*
[11] *Institute of Science and Technology Austria (ISTA), Am Campus 1, 3400 Klosterneuburg, Austria*
[12] *Max-Planck-Institut für Astronomie, Königstuhl 17, D-69117 Heidelberg, Germany*
[13] *Department of Natural Sciences, Faculty of Science and Engineering, Tokyo City University, 1-28-1 Tamazutsumi, Setagaya, Tokyo 158–8557, Japan*
[14] *Faculty of Industrial Technology, Tsukuba University of Technology, 4-3-15 Amakubo, Tsukuba, Ibaraki 305-8520, Japan*
[15] *Canadian Institute for Theoretical Astrophysics, 60 St George St, University of Toronto, Toronto, ON M5S 3H8, Canada*
[16] *David A. Dunlap Department of Astronomy and Astrophysics, University of Toronto, 50 St George St, Toronto ON M5S 3H4, Canada*
[17] *Department of Physics, 60 St George St, University of Toronto, Toronto, ON M5S 3H8, Canada*
[18] *Institute for Astronomy, School of Physics, Zhejiang University, Hangzhou 310058, Zhejiang, China*
[19] *Center for Cosmology and Computational Astrophysics, Zhejiang University, Hangzhou 310058, Zhejiang, China*

ABSTRACT

The James Webb Space Telescope (JWST) has uncovered a previously unexplored population of faint active galactic nuclei (AGNs) in the early Universe. We present MoM-BL-z10 at $z = 9.9837 \pm 0.0009$, identified through a systematic search for broad-line AGNs at $z \geq 6$ using public JWST/NIRSpec PRISM spectra from the DAWN JWST Archive. The PRISM spectrum exhibits a broad component in Hβ at 5.35 μm. A narrow+broad Gaussian fit yields a broad Hβ detection at S/N = 3.87, with FWHM $= 3480^{+2040}_{-950}$ km s^{-1} and $L_{\mathrm{H}\beta,\mathrm{broad}} = 1.25^{+0.33}_{-0.31} \times 10^{42}$ erg s^{-1}. The detection of [Ne III] λ3870 and the high [Ne III]/[O II] and [O III]/Hβ ratios further support the AGN interpretation. Its rest-frame UV and optical continuum slopes, compact NIRCam morphology, and a tentative MIRI F770W detection suggest similarities to Little Red Dots (LRDs). The broad Hβ detection enables the first virial SMBH mass estimate at $z \sim 10$. We derive $M_{\mathrm{BH}} = 3.6^{+5.8}_{-1.7} \times 10^7\ M_\odot$ and $\lambda_{\mathrm{Edd}} = 0.11^{+0.10}_{-0.07}$ using the standard single-epoch virial calibration and quasar bolometric correction. We also consider an alternative scenario adopting the LRD-specific bolometric correction and assuming $\lambda_{\mathrm{Edd}} = 1$, which yields $M_{\mathrm{BH}} = 2.1^{+0.6}_{-0.5} \times 10^6\ M_\odot$. Under either scenario, the inferred SMBH mass at a cosmic age of only 470 Myr highlights the challenge of rapid BH growth in the early Universe, suggesting super-Eddington accretion from a stellar-mass seed or a more massive seed. As the highest-redshift broad-line AGN identified to date, MoM-BL-z10 provides a new observational benchmark for understanding the early growth of supermassive black holes.

Email: xingyaocai@fuji.waseda.jp

Keywords: Active galactic nuclei (16) — High-redshift galaxies (734) — James Webb Space Telescope (2291)

1. INTRODUCTION

The existence of luminous quasars powered by billion-solar-mass black holes within the first billion years poses a major challenge to our understanding of the early growth history of SMBHs (X. Fan et al. 2023). Wide-field optical and near-infrared surveys have identified hundreds of luminous quasars down to $z = 7.8$ (e.g., E. Bañados et al. 2018; J. Yang et al. 2020; F. Wang et al. 2021; D. Yang et al. 2026). These luminous quasars place stringent constraints on seed BH formation and the rapid accretion histories of the rarest and most extreme population. However, those identified in wide-field surveys are limited to the bolometric luminosity range of $L_{\rm bol} \gtrsim 10^{46}$ erg s^{-1} (M. Onoue et al. 2019; C. J. Willott et al. 2010). Fainter and therefore less massive populations of active galactic nuclei (AGNs) are essential to investigate the buildup of the more representative SMBH population in the early universe.

The unprecedented infrared sensitivity of the James Webb Space Telescope (JWST; J. Rigby et al. 2023) enables us to probe the luminosity regime of Seyfert galaxies ($L_{\rm bol} \gtrsim 10^{44}$ erg s^{-1}) at high redshift. This new high-redshift AGN population has been identified via spectroscopic detection of broad Balmer emission lines (e.g., M. Onoue et al. 2023; D. D. Kocevski et al. 2023; Y. Harikane et al. 2023; V. Kokorev et al. 2023; R. Maiolino et al. 2024a; I. Juodžbalis et al. 2026). Single-epoch BH mass estimates of these populations yield $M_{\rm BH} \sim 10^6$–10^8 $M_\odot$, which are more than an order of magnitude lower than those of pre-JWST studies.

Remarkably, a non-negligible fraction of the JWST-selected AGNs exhibits compact morphology with "V"-shape continuum colors between rest-frame UV and optical wavelengths. These objects, called Little Red Dots (LRDs; e.g., J. Matthee et al. 2024; J. E. Greene et al. 2024), often exhibit broad Balmer lines, indicating the presence of accreting BHs. However, alternative stellar and wind-based interpretations have also been proposed (J. Chisholm et al. 2026; D. Nandal & A. Loeb 2026; L. Zwick et al. 2026; F. Martins et al. 2026; R. P. Naidu et al. 2026a). Proposed explanations for their characteristic spectra include dust-obscured AGNs (A. Noboriguchi et al. 2023; J. E. Greene et al. 2024), compact galaxies dominated by dusty star formation (H. B. Akins et al. 2023, 2025) or evolved stellar populations (J. F. W. Baggen et al. 2024), and accreting BHs embedded in dense gas envelopes ("BH star" model; K. Inayoshi & R. Maiolino 2025; A. J. Taylor et al. 2025; R. P. Naidu et al. 2026b; A. Torralba et al. 2026a; A. de Graaff et al. 2026).

Extensive efforts have been made to explore this LRD population out to $z \sim 10$. Broad Hβ emission has been detected in several LRDs, including UNCOVER 20466 at $z = 8.50$ (V. Kokorev et al. 2023), CANUCS-LRD-z8.6 at $z = 8.63$ (R. Tripodi et al. 2025), and CAPERS-LRD-z9 at $z = 9.288$ (A. J. Taylor et al. 2025), indicating that these sources host broad-line (BL) AGNs. T. S. Tanaka et al. (2025) reported a photometric candidate for a $z \sim 10$ LRD. There are also a few AGN candidates at similar redshifts. UHZ1 at $z = 10.1$ was initially reported to show a hard X-ray excess (Á. Bogdán et al. 2023) and was subsequently spectroscopically confirmed at $z_{\rm spec} = 10.073$ (A. D. Goulding et al. 2023; F. Zou et al. 2026). GN-z11 at $z = 10.6$ was first identified as a Lyman-break galaxy (P. A. Oesch et al. 2016), and its possible AGN nature has been discussed based on rest-frame UV/optical emission-line diagnostics (R. Maiolino et al. 2024b). However, neither UHZ1 nor GN-z11 has a securely detected broad emission-line component in its JWST spectrum, and the nature of the putative AGN activity in these sources remains debated (J. Álvarez-Márquez et al. 2025; F. Zou et al. 2026; Z. Chen et al. 2026).

In this Letter, we report the discovery of MoM-BL-z10, a BL AGN with spectroscopic redshift of $z = 9.9837$. This object is identified by a systematic archival search of publicly available JWST/NIRSpec PRISM data for BL AGNs independently of imaging colors or compactness. We subsequently assess its LRD classification using the spectrum, NIRCam morphology and MIRI photometry. We adopt a flat ΛCDM cosmology with $H_0 = 70$ km s^{-1} Mpc^{-1}, $\Omega_{\rm M} = 0.3$, and $\Omega_\Lambda = 0.7$, and use AB magnitudes (J. B. Oke & J. E. Gunn 1983). All emission-line wavelengths are quoted in vacuum.

2. DATA AND ANALYSIS

Here we briefly describe our BL AGN search. A full description of the complete sample will be presented in X. Cai et al. in preparation.

We use the public Near-Infrared Spectrograph (NIRSpec; P. Jakobsen et al. 2022) PRISM spectra from the DAWN JWST Archive (DJA version 4.4; F. Valentino et al. 2023; K. E. Heintz et al. 2024; A. de Graaff et al. 2025)[20]. After removing the duplicated observations,

[20] https://dawn-cph.github.io/dja/

the parent sample comprises 1,247 sources with grade-3 robust spectroscopic redshifts at $6.0 \leq z_{\rm spec} \leq 10.3$, ensuring that H$\beta$ falls within NIRSpec spectral coverage. We do not apply any criteria based on photometric colors and compactness for the parent selection. To account for possible changes in continuum slopes associated with LRD-like spectra, we adopt a broken power-law model with a fixed break at $\lambda_{\rm br} = 3645$ Å. We use 19 fitting windows spanning rest-frame 1275–8150 Å, following `PyQSOFit` (H. Guo et al. 2018; Y. Shen et al. 2019) with slight modifications (X. Cai et al. in preparation). After subtracting the continuum, we compare narrow-only and narrow+broad Gaussian models of Hβ+[O III]$\lambda\lambda$4960, 5008 complex and, when covered, Hα+[N II]$\lambda\lambda$6550, 6585 complex. The emission-line models are convolved with the wavelength-dependent NIRSpec line spread function (LSF) of P. Jakobsen et al. (2022), and adopt an effective resolving power 1.4 times the pre-launch estimate (A. de Graaff et al. 2024).

We use the Bayesian Information Criterion (BIC) (G. Schwarz 1978) to select BL AGN candidates. The selection threshold is $\Delta{\rm BIC} \equiv {\rm BIC}_{\rm narrow+broad} - {\rm BIC}_{\rm narrow-only} < -6$, which is commonly interpreted as strong evidence for the narrow+broad model over the narrow-only model (R. E. Kass & A. E. Raftery 1995). This threshold is also consistent with recent JWST BL AGN searches (J. E. Greene et al. 2024; J. Matthee et al. 2024; D. D. Kocevski et al. 2023; R. Maiolino et al. 2024a). We refine the model fit to the emission-line complex for BIC-selected candidates using `emcee` Markov chain Monte Carlo sampling (D. Foreman-Mackey et al. 2013), adding a 5% absolute flux-calibration uncertainty in quadrature to the statistical errors (K. D. Gordon et al. 2022; T. Böker et al. 2023) and adopt the posterior medians and 16th–84th percentiles. We define the BL S/N as the median flux divided by the mean of its lower and upper 68% uncertainties; requiring S/N ≥ 3 leaves 66 candidates. MoM-BL-z10 satisfies these criteria and is investigated below. Full details of the selection and the BL AGN catalog will be presented in a companion paper (X. Cai et al. in preparation).

3. MoM-BL-z10: A $z = 10$ BROAD-LINE AGN

3.1. *Emission Line Measurements*

MoM-BL-z10 is the highest-redshift source in our catalog. The NIRSpec MSA PRISM/CLEAR observations were obtained as part of the "Mirage or Miracle" (MoM) program (GO 5224; PIs: P.A. Oesch and R.P. Naidu; R. P. Naidu et al. 2026c), with a total effective exposure time of 15,756 s. Figure 1 shows its NIRSpec and NIRCam data (Section 3.2). MoM-BL-z10 exhibits a broad Hβ emission line at 5.35 μm, which is beyond the cutoff wavelength of the standard JWST pipeline (5.3 μm). This detection was made possible by the DJA data reduction that recovers second and third-order spectra (F. Valentino et al. 2025; C. L. Pollock et al. 2026). We obtain the systemic redshift of $z_{\rm spec} = 9.9837 \pm 0.0009$ by jointly fitting narrow optical emission lines including [O II] $\lambda\lambda$3727, 3730, [Ne III] $\lambda\lambda$3870, 3969, and [O III] λ4960. We note that only the blue edge of [O III] λ5008 is covered by the PRISM data, and we do not use it in our analysis.

The presence of a broad component in Hβ is statistically preferred, as the narrow+broad line model returns a smaller BIC relative to the narrow-line-only model ($\Delta{\rm BIC} = -15.55$). The decomposed narrow and broad Hβ fluxes are $F_{\rm H\beta,broad} = 93.4^{+24.9}_{-23.3} \times 10^{-20}\,{\rm erg\,s^{-1}\,cm^{-2}}$ and $F_{\rm H\beta,narrow} = 51.9^{+10.0}_{-10.3} \times 10^{-20}\,{\rm erg\,s^{-1}\,cm^{-2}}$, respectively. The corresponding detection significance of the broad line is S/N = 3.87. The intrinsic broad Hβ width is FWHM $= 3480^{+2040}_{-950}$ km s^{-1}, after correcting for instrumental broadening. There is a marginal velocity redshift of $604^{+449}_{-429}\,{\rm km\,s^{-1}}$ relative to the narrow lines. Here positive and negative velocity offsets indicate redshifted and blueshifted, respectively. The best-fit emission-line model and the reduction in the fit residuals achieved by including the broad Hβ component are shown in the rightmost middle panel of Figure 1.

For weaker emission lines, we measure their fluxes by integrating the continuum-subtracted spectrum over a wavelength window twice the width of the instrumental LSF, centered at the expected wavelengths based on the systemic redshift. Adopting a detection threshold of S/N ≥ 3, we detect the Hγ+[O III] λ4364 complex (S/N = 5.49), Si II] λ1817 (3.22), [O II] λ3728 (5.53), [Ne III] λ3869 (5.04), and [Ne III] λ3968+Hϵ (3.67). Their measured fluxes are listed in Table 1. We note that, for Hγ+[O III], we report the total flux over 4.755–4.807 μm. The narrow spike at ≈ 4.72 μm is not included in this wavelength window. We do not report the line profiles of these weak lines, given their low detection significance and the low spectral resolution of the PRISM data. We also find tentative evidence for C III] λ1909 (S/N = 2.86) and the He II λ1640+O III] λ1663 complex (2.18), despite their low detection significance. Other major AGN emission lines such as C IV λ1549 and Mg II λ2798 are not significantly detected.

We highlight that MoM-BL-z10 at $z = 9.98$ represents the highest-redshift broad-line AGN currently known, beyond CAPERS-LRD-z9 at $z = 9.29$ (A. J. Taylor et al. 2025), while luminous quasars are known down to $z = 7.77$ (D. Yang et al. 2026). The redshift of MoM-BL-z10 approaches the upper limit for detecting

Table 1. Observed and inferred properties of MoM-BL-z10

Property [unit]	Measurement
R.A. (ICRS) [dd:mm:ss][a]	02:17:07.229
Decl. (ICRS) [dd:mm:ss][a]	-05:09:38.63
Redshift	9.9837 ± 0.0009
f_ν(F090W) [nJy]	< 20.8
f_ν(F115W) [nJy]	< 20.3
f_ν(F150W) [nJy]	< 16.3
f_ν(F200W) [nJy]	31.5 ± 4.6
f_ν(F277W) [nJy]	14.6 ± 3.6
f_ν(F356W) [nJy]	9.9 ± 3.4
f_ν(F444W) [nJy]	18.1 ± 5.3
f_ν(F770W) [μJy]	0.20 ± 0.06
f_ν(F1280W) [μJy]	< 9.79
f_ν(F1500W) [μJy]	< 5.20
f_ν(F1800W) [μJy]	< 6.18
M_{1450} [AB mag]	$-19.37^{+0.14}_{-0.13}$
$\beta_{\rm UV}$	-1.64 ± 0.21
$\beta_{\rm opt}$	0.94 ± 0.83
Broad Hβ flux[b] [10^{-20} erg s^{-1} cm^{-2}]	$93.4^{+24.9}_{-23.3}$
Narrow Hβ flux[b]	$51.9^{+10.0}_{-10.3}$
Broad Hβ FWHM [km s^{-1}]	3480^{+2040}_{-950} km s^{-1}
Narrow-line FWHM [km s^{-1}]	< 527 km s^{-1} (95%)
Broad Hβ velocity offset [c]	604^{+449}_{-429}
Si II] λ1817 flux[b]	57.1 ± 17.8
[O II] $\lambda\lambda$3727, 3730 flux[b]	28.2 ± 5.1
[Ne III] λ3870 flux[b]	27.1 ± 5.4
[Ne III] λ3969+Hϵ flux[b]	19.0 ± 5.2
Hγ+[O III] λ4364 flux[b]	46.8 ± 8.5
[O III] λ4960 flux[b]	149.3 ± 11.0
L_{5100} [10^{43} erg s^{-1}]	$5.4^{+1.5}_{-1.2}$
$M_{\rm BH}$ [10^7 $M_\odot$]	$3.6^{+5.8}_{-1.7}$
$L_{\rm bol}$ [10^{44} erg s^{-1}][d]	$5.0^{+1.4}_{-1.1}$
$\lambda_{\rm Edd}$[d]	$0.11^{+0.10}_{-0.07}$
$L_{\rm bol,LRD}$[d] [10^{44} erg s^{-1}]	$2.7^{+0.7}_{-0.6}$
$M_{\rm BH,LRD}$[d] [10^6 $M_\odot$]	$2.1^{+0.6}_{-0.5}$

Note—Quoted uncertainties are 1σ errors or 16th–84th percentile intervals. The NIRCam photometry is measured within a $d = 0.''5$ aperture and taken from the DJA catalog. Photometric upper limits are given at 3σ. Positive broad Hβ velocity offsets indicate redshifts relative to the systemic velocity defined by the narrow emission lines.

[a] The coordinates are based on the NIRSpec source position. We confirm that the NIRCam position is consistent within $0.''026$ of this position. All MIRI fluxes and upper limits are measured using forced aperture photometry centered on these coordinates (see text).

[b] Emission line flux in units of 10^{-20} erg s^{-1} cm^{-2}. Those for Balmer and [O III] emission lines are based on single Gaussian fits. We also report those weaker lines with S/N ≥ 3, for which the line flux is derived by directly integrating the continuum-subtracted spectrum.

[c] The broad-Hβ velocity offset is given in km s^{-1} relative to the narrow-line systemic redshift. Positive (negative) values indicate a redshift (blueshift).

[d] We adopt $L_{\rm bol} = 9.26 L_{5100}$ for the quasar case (G. T. Richards et al. 2006), while we use $L_{\rm bol} = 5 L_{5100}$ for the LRD case (J. E. Greene et al. 2026). The SMBH mass for the LRD case ($M_{\rm BH,LRD}$ assumes $\lambda_{\rm Edd} = 1$).

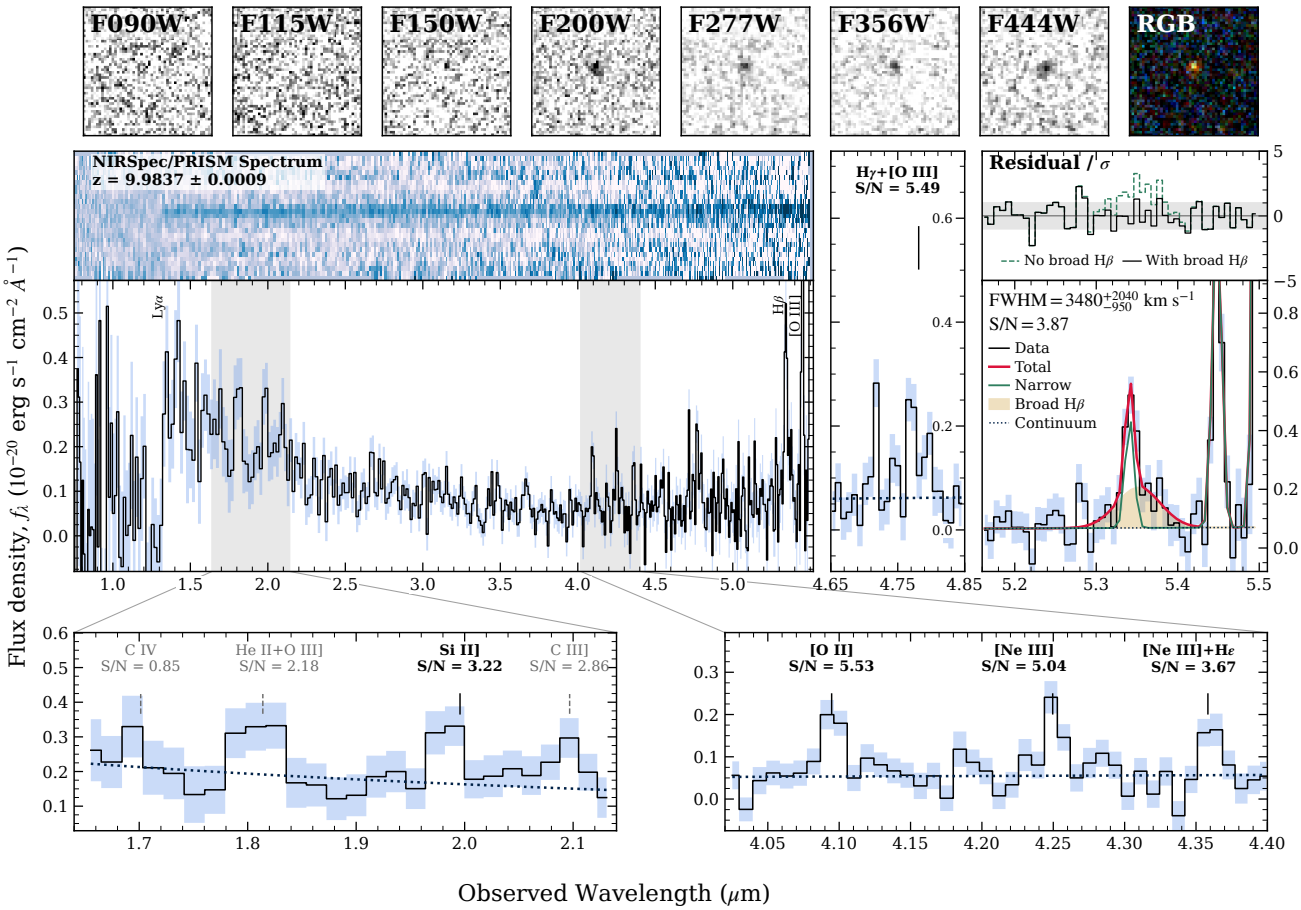


Figure 1. JWST spectroscopy and imaging of MoM-BL-z10. The top row shows 2×2 arcsec^2 cutout images in 7 NIRCam broadbands from F090W to F444W. The rightmost panel shows a pseudo-color image (blue: F090W+F115W+F150W; green: F200W+F277W; red: F356W+F444W). The middle panels show the 2D and 1D NIRSpec/PRISM spectra. In the 2D spectrum, positive and negative signals are shown in blue and white, respectively. The blue shaded region in the 1D spectrum indicates 1σ uncertainties. The positions of Lyα and Hβ+[O III] are marked. The right-hand panels show the Hγ+[O III] λ4364 and the Hβ+[O III] complex regions. In the Hβ+[O III] panel, we show the narrow+broad Gaussian fit to Hβ. The upper inset shows the normalized residuals for fits with and without the broad Hβ component. The bottom panels show zoomed-in views of weaker emission-line features, with labels in black for detections with S/N ≥ 3 and in gray for features with S/N < 3.

broad Hβ with the extended NIRSpec wavelength coverage (F. Valentino et al. 2025). Broad-line detection in higher-order Balmer emission lines would be more challenging (Hγ/Hβ=0.53; I. Juodžbalis et al. 2026). At $z \gtrsim 10$, AGN identification has largely relied on high-ionization or high-density emission-line diagnostics (e.g., GN-z11; R. Maiolino et al. 2024b; J. Álvarez-Márquez et al. 2025) or X-ray detections (e.g., UHZ1; A. D. Goulding et al. 2023; Á. Bogdán et al. 2023). However, GN-z11 at $z = 10.6$ does not show a dominant broad-Hα component in its MIRI/MRS spectrum (J. Álvarez-Márquez et al. 2025). Its optical emission is consistent with a metal-poor starburst, although a weak AGN contribution cannot be excluded (J. Álvarez-Márquez et al. 2025). For UHZ1, recent work also favors a low-mass, metal-poor, star-forming galaxy interpretation rather than a luminous obscured AGN (see e.g. F. Zou et al. 2026). There is a photometric candidate for a $z \sim 10$ LRD, CW-LRD-z10, reported in T. S. Tanaka et al. (2025), with MIRI follow-up spectroscopy scheduled under JWST-GO-9483.

3.2. *Continuum Measurements*

Multiple JWST programs (PRIMER, GO 1837, PI: J. Dunlop (C. T. Donnan et al. 2024); BEACON, GO 3990, PI: T. Morishita (T. Morishita et al. 2025) and GO 5324, PI: J. Pierel) observed MoM-BL-z10 with NIRCam. Seven broadband images are available in the DJA archive from F090W through F444W, which we present in the top panels of Figure 1. The source has a compact morphology, with an F444W aperture flux ratio of $f_{\rm F444W}(0\farcs50)/f_{\rm F444W}(0\farcs25) = 1.23 \pm 0.15$, measured using aperture diameters of $0\farcs50$ and $0\farcs25$. This satisfies the compactness criterion of $f_{\rm F444W}(0\farcs50)/f_{\rm F444W}(0\farcs25) < 1.7$ adopted in P. Rinaldi et al. (2025). We also perform independent aperture photometry using a $0\farcs20$-diameter aperture to find $f_{\rm F444W}(0\farcs50)/f_{\rm F444W}(0\farcs20) = 1.61 \pm 0.21$. This satisfies the compactness criterion of 1.4–2.0 adopted by T. S. Tanaka et al. (2025) for their $z > 10$ LRD selection.

Our continuum model based on the PRISM spectrum yields the rest-frame 1450 absolute magnitude of $M_{\rm UV} = -19.37^{+0.14}_{-0.13}$, which is similar to those of $z > 9$ BL AGNs (e.g., $M_{\rm UV} = -19.3$ for CANUCS-LRD-z9; T. Morishita et al. 2026), and about six magnitudes fainter than those of the luminous $z \sim 7.5$ quasars ($M_{1450} \sim -26$; E. Bañados et al. 2018; J. Yang et al. 2020; F. Wang et al. 2021).

MoM-BL-z10 exhibits a characteristic continuum shape in the rest-frame ultraviolet and optical wavelengths with the PRISM-based continuum slope measurements yielding $\beta_{\rm UV} = -1.64 \pm 0.21$ and $\beta_{\rm opt} = 0.94 \pm 0.83$. Although the optical slope is poorly constrained by the limited rest-frame wavelength coverage of the $z \approx 10$ source, at face value it satisfies the criteria for LRDs adopted in A. de Graaff et al. (2026).

We further investigate the rest-frame optical-and-infrared continuum colors with existing Mid-Infrared Instrument (MIRI; G. H. Rieke et al. 2015) imaging datasets in the target field, obtained through the PRIMER (GO 1837, PI: J. Dunlop; C. T. Donnan et al. 2024; P. G. Pérez-González et al. 2024) and MINERVA (GO 7814, PI: A. Muzzin; A. Muzzin et al. 2025) programs. The PRIMER observations cover the F770W and F1800W filters, with exposure times of 1,776 s and 1,787 s, respectively. The MINERVA observations provide F1280W and F1500W imaging, each with an exposure time of 760 s.

We report the multi-band photometry in Table 1. Figure 2 presents the NIRCam and MIRI photometric SED of MoM-BL-z10, together with the NIRSpec PRISM spectrum. For NIRCam, we adopt the photometry measured within a $0\farcs5$-diameter aperture from the DJA catalog (F. Valentino et al. 2023). Three-sigma upper limit fluxes are provided for the bands with S/N $\lesssim 3$. For MIRI, we perform aperture photometry using aperture diameters of $0\farcs602$ (F770W), $0\farcs860$ (F1280W), $1\farcs012$ (F1500W), and $1\farcs190$ (F1800W). These aperture diameters are set to twice the PSF FWHM in each band[21]. We estimate the background noise in the MIRI images using random apertures of the same size as those adopted for the source photometry, placed within a 10×10 arcsec^2 region centered on the source. As MoM-BL-z10 is located close to the boundaries of the MIRI imaging coverage, we mask pixels affected by edge artifacts in the background estimate. In the F1280W and F1500W images, the source is covered by fewer dither positions than the central regions, resulting in a shorter effective exposure time. To account for this reduced imaging depth, we restrict the random apertures to regions with the same dither coverage as the source. As a result, we find a tentative detection of MoM-BL-z10 in F770W with $f_\nu({\rm F770W}) = 0.20 \pm 0.06$ μJy (S/N = 3.33), while it is not significantly detected in the three redder filters. The 3σ upper limits in F1280W, F1500W, and F1800W are 9.79, 5.20 and 6.18 μJy, respectively.

We now revisit the continuum properties of MoM-BL-z10 using the additional constraints from MIRI photometry, although the F770W detection remains tentative. The measured NIRCam+MIRI colors, F277W − F444W $= 0.23 \pm 0.42$ and F444W − F770W $= 2.61 \pm$

[21] https://jwst-docs.stsci.edu/jwst-mid-infrared-instrument/miri-performance/miri-point-spread-functions

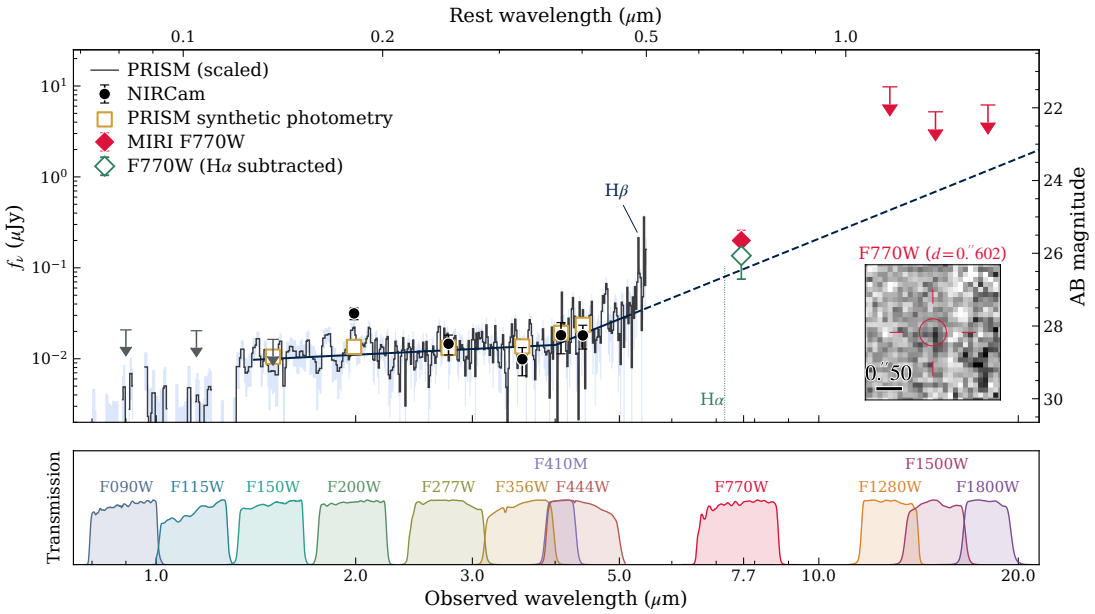


Figure 2. Rest-frame UV-to-near-infrared SED of MoM-BL-z10, combining NIRCam and MIRI photometry with a scaled PRISM spectrum (see text). For visualization, the PRISM spectrum is resampled onto a logarithmic wavelength grid with a fixed velocity step of $\Delta v = 1160$ km s^{-1}. Black circles show the NIRCam photometry, and grey arrows indicate the 3σ upper limits for undetected bands. Open orange squares show synthetic PRISM photometry, obtained by convolving the scaled PRISM spectrum with the NIRCam filter transmission curves. The filled diamond shows the tentative MIRI F770W detection. The open green diamond shows the estimated continuum flux after subtracting Hα contribution, assuming $L_{\rm H\alpha} = 10 L_{\rm H\beta}$. Red arrows indicate the 3σ upper limits of other MIRI bands. The thick solid lines show the broken-power-law continuum model, while the dashed line is the extrapolation to the MIRI coverage. The inset shows a 3×3 arcsec^2 F770W cutout image, where a red circle indicates the photometric aperture ($d = 0.''602$) centered on the source position. The transmission curves of the NIRCam and MIRI filters are shown in the bottom panel.

0.45 mag, are consistent with the expected colors of $z \sim 10$ LRDs. T. S. Tanaka et al. (2025) adopt color cuts of $0 <$ F277W $-$ F444W < 3.0 and F444W $-$ F770W > 1.5 to select their $z > 10$ LRD candidates, both of which are satisfied by MoM-BL-z10. Together with its relatively blue UV continuum slope and compact morphology (Section 3.2), these colors suggest that MoM-BL-z10 exhibits characteristics consistent with being a $z \approx 10$ LRD. Nevertheless, we refrain from classifying MoM-BL-z10 as an LRD from the current dataset, given the limited constraints on the rest-frame optical continuum shape and its low-detection significance in F770W (S/N = 3.33). Deeper NIRSpec data and/or MIRI imaging are needed to better constrain its continuum shape and establish its nature.

3.3. *Hα Contribution to F770W*

Redshifted Hα emission of MoM-BL-z10 falls at 7.21 μm, thus contributing to MIRI F770W photometry. To quantify this contribution, we first normalize the PRISM spectrum to the NIRCam photometry by comparing the synthetic broadband fluxes derived from the PRISM spectrum with the observed NIRCam fluxes. This yields a scaling factor of $s = 0.509 \pm 0.063$ (i.e., the PRISM spectrum is ≈ 2 times higher). Applying this scaling factor to the observed Hβ flux and assuming a Balmer decrement of $L_{\rm H\alpha}/L_{\rm H\beta} = 10$, as typically observed in LRDs (e.g., $H\alpha/H\beta = 10.4$ in X. Lin et al. 2026; A. Torralba et al. 2026b; A. de Graaff et al. 2026; T. Kiyota et al. 2026), we estimate an Hα contribution of 0.064 ± 0.012 μJy to F770W. Subtracting this contribution from the observed F770W photometry yields a residual flux density of 0.136 ± 0.061 μJy. The Hα-subtracted F770W flux, shown as an open green diamond in Figure 2, is consistent with the extrapolation of the single power-law model fitted to the rest-frame optical continuum of the PRISM spectrum. The marginal F770W detection is therefore consistent with the presence of a red rest-frame optical continuum in MoM-BL-z10.

4. DISCUSSION

4.1. *Emission Line Diagnostics*

The metal-line excitation provides a complementary check on the AGN interpretation of MoM-BL-z10. We obtain $\log([\mathrm{Ne\,III}]/[\mathrm{O\,II}]) = -0.016^{+0.231}_{-0.233}$, $\log([\mathrm{O\,III}]/[\mathrm{O\,II}]) = 1.199^{+0.091}_{-0.079}$, and $\log([\mathrm{O\,III}]/\mathrm{H}\beta_{\rm narrow}) = 0.933^{+0.103}_{-0.084}$. Here [Ne III] de-

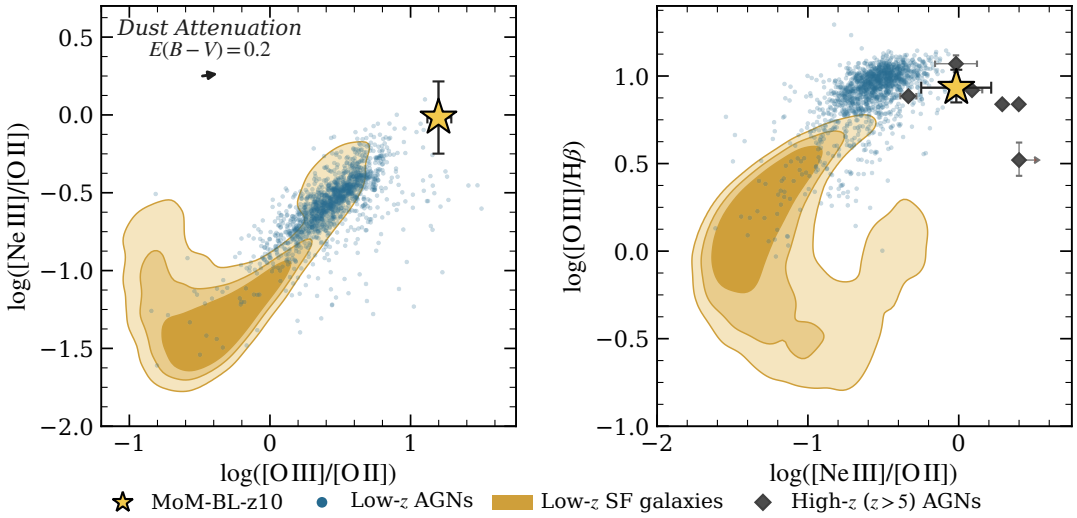


Figure 3. The [O II]-FLR (left) and OHNO (right) diagnostics. The yellow star shows MoM-BL-z10, where we infer the [O III] λ5008 from the [O III] λ4960 flux by assuming a fiducial flux ratio of 2.98, and only the narrow Hβ component is used. The error bars reflect the propagated 1σ measurement uncertainties of the emission-line fluxes. An additional 0.20-dex uncertainty is added in quadrature to log([Ne III]/[O II]) to account for possible blending with Hη, Hζ, and He I λ3889 (e.g., R. Tripodi et al. 2025). Blue points show the SDSS AGN sample selected from BPT and [Ne V] λ3426 emission in the Portsmouth SDSS galaxy-property catalogue (L. M. Feuillet et al. 2024); orange contours indicate 50, 70, and 90% of the density of low-redshift BPT-selected MPA–JHU SF galaxies from the MPA–JHU catalogue of SDSS DR8 galaxy spectra (J. Brinchmann et al. 2004; G. Kauffmann et al. 2003). Other symbols represent high-redshift ($z > 5$) JWST AGNs published in the literature (J. A. A. Trussler et al. 2023; R. Tripodi et al. 2024; H. Übler et al. 2024; D. Nandal et al. 2025; R. Tripodi et al. 2025; B. E. Backhaus et al. 2024). The arrow in the left panel indicates the effect of dust attenuation corresponding to $E(B-V) = 0.2$ mag, assuming the attenuation law of D. Calzetti et al. (2000).

notes λ3870, [O II] denotes the unresolved $\lambda\lambda$3727, 3730 doublet, and [O III]λ5008 is inferred from [O III]λ4960 using the theoretical ratio of 2.98 (P. J. Storey & C. J. Zeippen 2000). We propagate measurement errors and add an additional 0.20-dex [Ne III] blending uncertainty to the [Ne III]/[O II] ratio. This term accounts for possible contamination of [Ne III] by Hη, Hζ, and He I λ3889 at PRISM resolution, following the discussion of R. Tripodi et al. (2025).

Figure 3 compares MoM-BL-z10 in the [Ne III]/[O II] versus [O III]/[O II] ([O II]-forbidden line ratio, FLR) and [O III]/Hβ versus [Ne III]/[O II] (OHNO) diagrams. The AGN reference comprises SDSS galaxies from L. M. Feuillet et al. (2024), selected by BPT AGN classification and [Ne V] S/N > 3. The SF galaxies reference comprises around 40,000 MPA–JHU DR8 star-forming spectra (J. Brinchmann et al. 2004; D. Thomas et al. 2013)[22] with BPT lines below the G. Kauffmann et al. (2003) [N II]/Hα boundary.

MoM-BL-z10 lies in the AGN-like region in both diagnostics. In the [O II]-FLR diagram (left panel of Figure 3), high ratios in both axes can reflect a high ionization parameter or suppression of [O II] in dense gas (L. M. Feuillet et al. 2024). MoM-BL-z10 is beyond the SF contours, towards the high-excitation end of the low-z SDSS AGN distribution. The OHNO diagram (right panel of Figure 3) instead compares [O III] with narrow Hβ. MoM-BL-z10 also lies in the AGN distribution. For $E(B-V) = 0.2$, the D. Calzetti et al. (2000) dust correction still leaves MoM-BL-z10 outside of SF contours, so we exclude the dust attenuation as the explanation for its separation from the SF locus. We therefore identify MoM-BL-z10 as an AGN based on the combined evidence from its broad Hβ and its position in both line-ratio diagnostics.

4.2. *Black Hole Mass Estimate*

The broad Hβ detection of MoM-BL-z10 enables us to estimate its central black hole mass. We first estimate its virial black hole mass using the single-epoch calibration of S. Kaspi et al. (2000), based on rest-frame 5100 Å continuum luminosity (L_{5100}) and the broad Hβ FWHM. The observed continuum luminosity from the PRISM spectrum, without correction for possible host galaxy contamination and inconsistency between the NIRCam and NIRSpec data (Sec. 3.3), is $L_{5100} = 5.4^{+1.5}_{-1.2} \times 10^{43}$ erg s^{-1}. Combining this with the measured broad Hβ FWHM $= 3480^{+2040}_{-950}$ km s^{-1}, we obtain $M_{\rm BH} = 3.6^{+5.8}_{-1.7} \times 10^7 M_\odot$. We note that the

[22] https://www.sdss4.org/dr12/spectro/galaxy_portsmouth/

broad Hβ luminosity relative to the optical continuum is higher than expected from the relation observed in the local universe (J. E. Greene & L. C. Ho 2005), a trend generally seen in the broad-line emitters from our sample (X. Cai et al. in preparation). The same trend has also been reported for other high-redshift AGN samples (e.g., A. de Graaff et al. 2026; H. Yanagisawa et al. 2026; M. Onoue et al. 2026). We therefore adopt the continuum-based virial mass calibration rather than one based on the broad Balmer luminosity. Applying the quasar bolometric correction $L_{\rm bol} = 9.26\ L_{5100}$ (G. T. Richards et al. 2006), we estimate an AGN bolometric luminosity of $L_{\rm bol} = 5.0^{+1.4}_{-1.1} \times 10^{44}$ erg s^{-1}. The corresponding Eddington ratio, $\lambda_{\rm Edd} \equiv L_{\rm bol}/L_{\rm Edd}$, is $\lambda_{\rm Edd} = 0.11^{+0.10}_{-0.07}$.

Given the red optical continuum and compact morphology of MoM-BL-z10 (Sec. 3.2), we also consider an alternative interpretation motivated by recent LRD studies. Adopting the LRD bolometric correction of $L_{\rm bol,LRD} = 5L_{5100}$ (J. E. Greene et al. 2026), which is approximately half the standard value for quasars, we obtain $L_{\rm bol,LRD} = 2.7^{+0.7}_{-0.6} \times 10^{44}$ erg s^{-1}. Recent LRD models suggest that SMBHs may undergo near- or super-Eddington accretion during the LRD phase (R. P. Naidu et al. 2026a; W. Q. Sun et al. 2026; O. Curtis et al. 2026). Motivated by these studies, we consider an illustrative case of Eddington-limited accretion ($\lambda_{\rm Edd} = 1$) for MoM-BL-z10. Combining this assumption with the LRD-specific bolometric luminosity, we obtain $M_{\rm BH,LRD} = 2.1^{+0.6}_{-0.5} \times 10^6\ M_\odot$, which is approximately 17 times smaller than our fiducial virial BH mass estimate. The quoted mass uncertainty reflects only the uncertainty in L_{5100}. Figure 4 compares these two cases with other $z \gtrsim 8$ AGNs in the SMBH mass – bolometric luminosity plane.

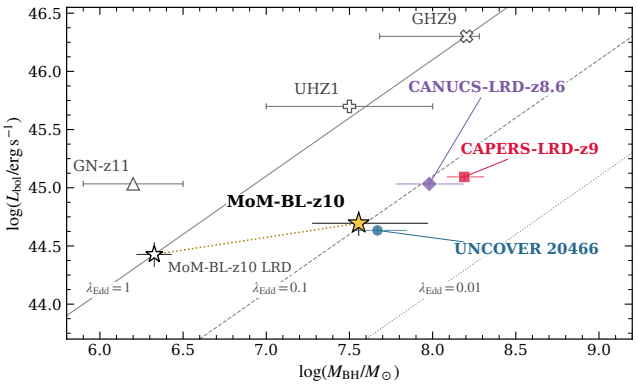


Figure 4. Black hole mass–bolometric luminosity distribution at $z \gtrsim 8$. The yellow star shows MoM-BL-z10 with the black hole mass estimated using the Hβ-based calibration of S. Kaspi et al. (2000) and the standard bolometric correction for quasars ($L_{\rm bol} = 9.26 L_{5100}$; G. T. Richards et al. 2006). The white star shows the alternative LRD case for the same object, adopting the bolometric correction of $L_{\rm bol,LRD} = 5L_{5100}$ (J. E. Greene et al. 2026) and assuming an Eddington-limited accretion ($\lambda_{\rm Edd} = 1$). In the LRD-based $M_{\rm BH}$ estimate, only the uncertainty of continuum luminosity is considered in the error budget, whereas the fiducial virial $M_{\rm BH}$ uncertainty includes those in both L_{5100} and broad Hβ FWHM. The black hole mass and bolometric luminosity of other $z \gtrsim 8$ BL AGNs (CAPERS-LRD-z9 (A. J. Taylor et al. 2025), UNCOVER 20466 (V. Kokorev et al. 2023), and CANUCS-LRD-z8.6 (R. Tripodi et al. 2025)) are re-measured with the same procedure as for MoM-BL-z10 using the GH05 relation (J. E. Greene & L. C. Ho 2005). Open symbols show $z > 9$ AGNs without broad line detection; GN-z11 (R. Maiolino et al. 2024b), UHZ1 (Á. Bogdán et al. 2023), and GHZ9 (L. Napolitano et al. 2025). We adopt $M_{\rm BH}$ and $L_{\rm bol}$ reported in the original papers. Diagonal lines indicate Eddington ratios of $\lambda_{\rm Edd} = 1$, 0.1, and 0.01 from upper left to bottom right.

4.3. *Implications for Early Black Hole Growth*

The inferred SMBH mass of MoM-BL-z10 at $z = 9.98$ provides a valuable constraint on early SMBH growth. Figure 5 illustrates the mass growth history of MoM-BL-z10 as a function of redshift, where we assume a seed formation epoch of $z = 25$ and continuous accretion with a 10% radiation efficiency (Q. Yu & S. Tremaine 2002; A. Marconi et al. 2004). For our fiducial virial mass estimate of $M_{\rm BH} = 3.6 \times 10^7\ M_\odot$, growth from stellar-mass BH seeds ($M_{\rm seed} \sim 10$–$100\ M_\odot$; P. Madau & M. J. Rees 2001; Z. Haiman & A. Loeb 2001; A. Heger et al. 2003) requires a time-averaged Eddington ratio of $\lambda_{\rm Edd} \approx 2$. This echoes the well-known challenge of explaining the existence of massive SMBHs at $z \gtrsim 7$ (D. J. Mortlock et al. 2011; E. Bañados et al. 2018; F. Wang et al. 2021; D. Yang et al. 2026), as is also indicated by the darker blue curve in Figure 5, where we assume $\lambda_{\rm Edd} = 1$. Indeed, under a heavy-seed scenario ($M_{\rm seed} \sim 10^{4-5} M_\odot$), continuous Eddington-limited accretion can produce both the inferred SMBH mass of MoM-BL-z10, and those of luminous quasars at $z \gtrsim 7$ and other known JWST AGN at $z \gtrsim 8$ (A. J. Taylor et al. 2025; V. Kokorev et al. 2023; R. Tripodi et al. 2025). Such massive BH seeds may form through the direct collapse of pristine gas clouds (G. Lodato & P. Natarajan 2006; M. A. Latif et al. 2022) or through runaway stellar collisions in dense star clusters (M. Gieles et al. 2018; C. E. Williams et al. 2026; A. Rantala 2026).

We note that the fiducial Eddington ratio of $\lambda_{\rm Edd} = 0.11$ reflects the accretion state at the observed epoch and would be insufficient to explain the inferred BH mass if maintained since $z = 25$ under our growth assumptions, as illustrated by the yellow stripe in Figure 5. It is therefore more plausible that MoM-BL-z10 experi-

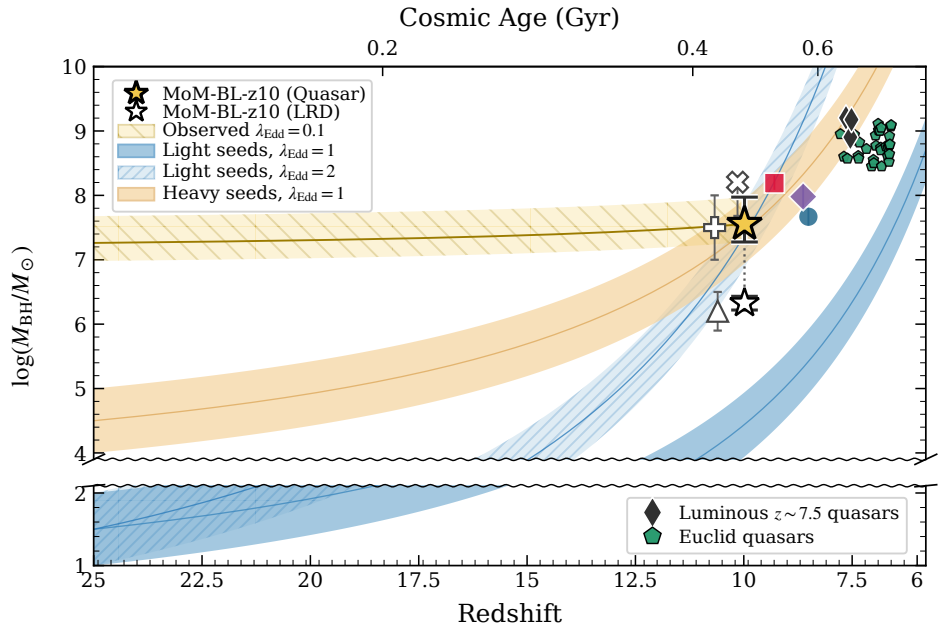


Figure 5. Illustrative black hole growth tracks of MoM-BL-z10 as a function of redshift assuming continuous accretion at fixed Eddington ratios with 10% radiative efficiency. The yellow star shows the fiducial virial SMBH mass of MoM-BL-z10, while the white star shows the LRD-based SMBH mass estimate assuming Eddington-limited accretion. The yellow stripe shows the backward extrapolation of the fiducial BH mass, assuming the observed Eddington ratio of $\lambda_{\rm Edd} = 0.1$. The orange and blue stripes show the expected growth curves from a heavy (10^{4-5} $M_\odot$) and a light (10–100 $M_\odot$) seed BH, respectively, assuming continuous Eddington-limited accretion ($\lambda_{\rm Edd} = 1$) beginning at $z = 25$. The widths of these stripes correspond to their seed mass ranges. The lighter, hatched blue stripe shows the same light-seed track for a super-Eddington accretion case ($\lambda_{\rm Edd} = 2$). Other symbols show known high-redshift quasars and AGNs in the literature; $z \sim 7.5$ luminous quasars (diamonds; F. Wang et al. 2021; E. Bañados et al. 2018; J. Yang et al. 2020), Euclid quasars (pentagons; D. Yang et al. 2026), and JWST AGNs shown in Figure 4 with the same symbols. UHZ1 is shifted by $\Delta z = +0.6$ from its spectroscopic redshift for clarity. For the Euclid quasars, black hole masses are estimated from their bolometric luminosities assuming $\lambda_{\rm Edd} = 0.25$, the median value of the comparably luminous $z \sim 6$ quasars (M. Onoue et al. 2026).

enced more rapid accretion in the past, potentially including episodes of near- or super-Eddington accretion (W. Li et al. 2024).

Under the alternative LRD interpretation discussed in Section 4.2, the inferred BH mass of MoM-BL-z10 decreases to $M_{\rm BH,LRD} = 2.1\times10^6$ $M_\odot$, substantially relaxing the requirements for early BH growth. Nevertheless, given the limited time available for BH growth, even this lower mass is still challenging to explain through continuous Eddington-limited accretion from stellar-mass BH seeds (Figure 5).

5. CONCLUSIONS

We report the discovery of MoM-BL-z10, the highest-redshift broad-line AGN currently known at $z = 9.98$, identified through our systematic search for broad-line AGNs at $6 < z < 10$ using archival JWST/NIRSpec PRISM spectra. A full description of the survey will be presented in X. Cai et al. (in preparation). Our main conclusions are as follows:

1. MoM-BL-z10 at $z = 9.98$ is the highest-redshift object in our broad-line AGN sample, selected solely on the basis of NIRSpec/PRISM spectroscopy of 1,247 objects at $6.0 \leq z \leq 10.3$ without photometric pre-selection. The Hβ emission-line profile of MoM-BL-z10 is well reproduced by a model consisting of narrow and broad Gaussian components, with the narrow component constrained by the [O III] λ4960 line profile. The BIC favors this model over a narrow-line-only model with ΔBIC $= -15.55$. The broad Hβ component is detected at S/N $= 3.87$, with FWHM $= 3480^{+2040}_{-950}$ km s^{-1}.

2. The AGN interpretation of MoM-BL-z10 is further supported by its compact morphology in F444W, and the detection of strong [O III] λ4960 and [Ne III] λ3869 emission. The high-excitation emission-line ratios place MoM-BL-z10 in the AGN-like regions of both the [O II]-FLR and OHNO diagnostic diagrams, well separated from the loci of star-forming galaxies.

3. The rest-frame UV and optical slopes of MoM-BL-z10 are consistent with a $z = 10$ LRD, albeit with a large uncertainty in $\beta_{\rm opt}$ ($= 0.94 \pm 0.83$). We also find a tentative detection (S/N = 3.3) in MIRI F770W, which, if real, lends further support to its LRD-like nature.

4. We estimate the AGN bolometric luminosity of MoM-BL-z10 as $L_{\rm bol} = 4.95^{+1.39}_{-1.09} \times 10^{44}$ erg s^{-1}, adopting the standard quasar bolometric correction. Using the rest-frame 5100 Å continuum luminosity and broad Hβ line width, we derive a virial BH mass of $M_{\rm BH} = 3.59^{+5.79}_{-1.71} \times 10^7\ M_\odot$ and an Eddington ratio of $\lambda_{\rm Edd} = 0.11^{+0.10}_{-0.07}$. Alternatively, adopting the LRD-specific bolometric correction and assuming Eddington-limited accretion ($\lambda_{\rm Edd} = 1$) yields an illustrative BH mass estimate of $M_{\rm BH,LRD} = 2.1 \times 10^6\ M_\odot$.

The broad Hβ emission in MoM-BL-z10 lies near the long-wavelength limit of the extended NIRSpec/PRISM coverage, while broad Hα would be challenging to detect with MIRI due to its lower sensitivity. Thus, the redshift of MoM-BL-z10 may be close to the practical redshift limit for identifying faint AGNs through broad Balmer emission with JWST. Extending systematic spectroscopic searches to larger samples with well-characterized selection functions will help establish how common these early AGNs are and provide further constraints on BH formation and growth.

Observed at $z = 9.98$, when the Universe was only 470 Myr old, MoM-BL-z10 represents the highest-redshift broad-line AGN with an Hβ-based virial BH mass estimate, bringing into sharper focus the long-standing challenge of understanding rapid SMBH growth in the early Universe.

ACKNOWLEDGMENTS

This work is based on observations made with the NASA/ESA/CSA James Webb Space Telescope. The MIRI data were obtained from the Mikulski Archive for Space Telescopes at the Space Telescope Science Institute, which is operated by the Association of Universities for Research in Astronomy, Inc., under NASA contract NAS 5-03127 for JWST. The specific observations analyzed can be accessed via https://doi.org/10.17909/sngr-7t73. The NIRSpec data products presented herein were retrieved from the Dawn JWST Archive (DJA). DJA is an initiative of the Cosmic Dawn Center (DAWN), which is funded by the Danish National Research Foundation under grant DNRF140.

RPN acknowledges support from JWST-GO-5224. JM acknowledges funding by the European Union (ERC, AGENTS, 101076224). KM acknowledges support from the Waseda University Grant for Special Research Projects (Project Number 2025C-484). AdG acknowledges funding by the European Union (ERC, FIRST-GIANTS, 101221926). AdG is supported by the Lise Meitner Excellence program of the Max Planck Society. PD warmly acknowledges support from an NSERC discovery grant (RGPIN-2025-06182). This work is supported by JSPS KAKENHI Grant Numbers JP23K13149, 26K00736, 26K07155, 26H02069, JP26K17200 and 26K07139. This work has received funding from the Swiss State Secretariat for Education, Research and Innovation (SERI) under contract number MB22.00072, as well as from the Swiss National Science Foundation (SNSF) through project grants 200020_207349 and 2000-1-243073. XC thanks John D. Silverman and Takumi S. Tanaka for insightful discussions.

AUTHOR CONTRIBUTIONS

X. C. conducted the investigation and prepared the initial draft of the manuscript. A. K. I., M. O., and Y. F. developed the initial idea and research goals. A. K. I. provided primary supervision and mentorship. M. O. provided additional supervision and methodological guidance, and took a leading role in reviewing and editing the manuscript. S. A. contributed to the investigation and discussion of the results. All authors contributed to reviewing and editing the manuscript.

Facilities: JWST(NIRSpec, NIRCam, MIRI)

Software: Astropy (Astropy Collaboration et al. 2013, 2018, 2022), `emcee` (D. Foreman-Mackey et al. 2013), `lmfit` (M. Newville et al. 2014), Matplotlib (J. D. Hunter 2007), NumPy (C. R. Harris et al. 2020), SciPy (P. Virtanen et al. 2020)

REFERENCES

Akins, H. B., Casey, C. M., Allen, N., et al. 2023, ApJ, 956, 61, doi: 10.3847/1538-4357/acef21

Akins, H. B., Casey, C. M., Lambrides, E., et al. 2025, ApJ, 991, 37, doi: 10.3847/1538-4357/ade984

Álvarez-Márquez, J., Crespo Gómez, A., Colina, L., et al. 2025, A&A, 695, A250, doi: 10.1051/0004-6361/202451731

Astropy Collaboration, Robitaille, T. P., Tollerud, E. J., et al. 2013, A&A, 558, A33, doi: 10.1051/0004-6361/201322068

Astropy Collaboration, Price-Whelan, A. M., Sipőcz, B. M., et al. 2018, AJ, 156, 123, doi: 10.3847/1538-3881/aabc4f

Astropy Collaboration, Price-Whelan, A. M., Lim, P. L., et al. 2022, ApJ, 935, 167, doi: 10.3847/1538-4357/ac7c74

Bañados, E., Venemans, B. P., Mazzucchelli, C., et al. 2018, Nature, 553, 473, doi: 10.1038/nature25180

Backhaus, B. E., Trump, J. R., Pirzkal, N., et al. 2024, ApJ, 962, 195, doi: 10.3847/1538-4357/ad1520

Baggen, J. F. W., van Dokkum, P., Brammer, G., et al. 2024, ApJL, 977, L13, doi: 10.3847/2041-8213/ad90b8

Bogdán, Á., Goulding, A. D., Natarajan, P., et al. 2023, Nature Astronomy, 8, 126, doi: 10.1038/s41550-023-02111-9

Brinchmann, J., Charlot, S., White, S. D. M., et al. 2004, MNRAS, 351, 1151, doi: 10.1111/j.1365-2966.2004.07881.x

Böker, T., Beck, T. L., Birkmann, S. M., et al. 2023, Publications of the Astronomical Society of the Pacific, 135, 038001, doi: 10.1088/1538-3873/acb846

Calzetti, D., Armus, L., Bohlin, R. C., et al. 2000, ApJ, 533, 682, doi: 10.1086/308692

Chen, Z., Stark, D. P., Mason, C. A., et al. 2026, arXiv e-prints, arXiv:2604.21516, doi: 10.48550/arXiv.2604.21516

Chisholm, J., Berg, D. A., Boylan-Kolchin, M., et al. 2026, ApJL, 1004, L4, doi: 10.3847/2041-8213/ae6dae

Curtis, O., Cleri, N. J., Helton, J. M., Leja, J., & Wright, J. T. 2026, arXiv e-prints, arXiv:2609.09265, doi: 10.48550/arXiv.2609.09265

de Graaff, A., Rix, H.-W., Carniani, S., et al. 2024, A&A, 684, A87, doi: 10.1051/0004-6361/202347755

de Graaff, A., Brammer, G., Weibel, A., et al. 2025, A&A, 697, A189, doi: 10.1051/0004-6361/202452186

de Graaff, A., Hviding, R. E., Naidu, R. P., et al. 2026, MNRAS, 551, stag1567, doi: 10.1093/mnras/stag1567

Donnan, C. T., McLure, R. J., Dunlop, J. S., et al. 2024, MNRAS, 533, 3222, doi: 10.1093/mnras/stae2037

Fan, X., Bañados, E., & Simcoe, R. A. 2023, ARA&A, 61, 373, doi: 10.1146/annurev-astro-052920-102455

Feuillet, L. M., Meléndez, M., Kraemer, S., et al. 2024, ApJ, 962, 104, doi: 10.3847/1538-4357/ad1a09

Foreman-Mackey, D., Hogg, D. W., Lang, D., & Goodman, J. 2013, PASP, 125, 306, doi: 10.1086/670067

Gieles, M., Charbonnel, C., Krause, M. G. H., et al. 2018, MNRAS, 478, 2461, doi: 10.1093/mnras/sty1059

Gordon, K. D., Bohlin, R., Sloan, G. C., et al. 2022, The Astronomical Journal, 163, 267, doi: 10.3847/1538-3881/ac66dc

Goulding, A. D., Greene, J. E., Setton, D. J., et al. 2023, ApJL, 955, L24, doi: 10.3847/2041-8213/acf7c5

Greene, J. E., & Ho, L. C. 2005, ApJ, 630, 122, doi: 10.1086/431897

Greene, J. E., Labbe, I., Goulding, A. D., et al. 2024, The Astrophysical Journal, 964, 39, doi: 10.3847/1538-4357/ad1e5f

Greene, J. E., Setton, D. J., Furtak, L. J., et al. 2026, ApJ, 996, 129, doi: 10.3847/1538-4357/ae1836

Guo, H., Shen, Y., & Wang, S. 2018, PyQSOFit: Python code to fit the spectrum of quasars„ Astrophysics Source Code Library, record ascl:1809.008 http://ascl.net/1809.008

Haiman, Z., & Loeb, A. 2001, ApJ, 552, 459, doi: 10.1086/320603

Harikane, Y., Zhang, Y., Nakajima, K., et al. 2023, The Astrophysical Journal, 959, 39, doi: 10.3847/1538-4357/ad029e

Harris, C. R., Millman, K. J., van der Walt, S. J., et al. 2020, Nature, 585, 357, doi: 10.1038/s41586-020-2649-2

Heger, A., Fryer, C. L., Woosley, S. E., Langer, N., & Hartmann, D. H. 2003, ApJ, 591, 288, doi: 10.1086/375341

Heintz, K. E., Watson, D., Brammer, G., et al. 2024, Science, 384, 890, doi: 10.1126/science.adj0343

Hunter, J. D. 2007, Computing in Science and Engineering, 9, 90, doi: 10.1109/MCSE.2007.55

Inayoshi, K., & Maiolino, R. 2025, ApJL, 980, L27, doi: 10.3847/2041-8213/adaebd

Jakobsen, P., Ferruit, P., Alves de Oliveira, C., et al. 2022, A&A, 661, A80, doi: 10.1051/0004-6361/202142663

Juodžbalis, I., Maiolino, R., Baker, W. M., et al. 2026, MNRAS, 546, stag086, doi: 10.1093/mnras/stag086

Kaspi, S., Smith, P. S., Netzer, H., et al. 2000, ApJ, 533, 631, doi: 10.1086/308704

Kass, R. E., & Raftery, A. E. 1995, Journal of the American Statistical Association, 90, 773, doi: 10.1080/01621459.1995.10476572

Kauffmann, G., Heckman, T. M., White, S. D. M., et al. 2003, MNRAS, 341, 33, doi: 10.1046/j.1365-8711.2003.06291.x

Kiyota, T., Ouchi, M., Yanagisawa, H., et al. 2026, arXiv e-prints, arXiv:2608.10832, doi: 10.48550/arXiv.2608.10832

Kocevski, D. D., Onoue, M., Inayoshi, K., et al. 2023, arXiv e-prints, arXiv:2302.00012, doi: 10.48550/arXiv.2302.00012
Kokorev, V., Fujimoto, S., Labbe, I., et al. 2023, The Astrophysical Journal Letters, 957, L7, doi: 10.3847/2041-8213/ad037a
Latif, M. A., Whalen, D. J., Khochfar, S., Herrington, N. P., & Woods, T. E. 2022, Nature, 607, 48, doi: 10.1038/s41586-022-04813-y
Li, W., Inayoshi, K., Onoue, M., et al. 2024, ApJ, 969, 69, doi: 10.3847/1538-4357/ad46f9
Lin, X., Fan, X., Wang, F., et al. 2026, ApJ, 996, 93, doi: 10.3847/1538-4357/ae1b9b
Lodato, G., & Natarajan, P. 2006, MNRAS, 371, 1813, doi: 10.1111/j.1365-2966.2006.10801.x
Madau, P., & Rees, M. J. 2001, ApJL, 551, L27, doi: 10.1086/319848
Maiolino, R., Scholtz, J., Curtis-Lake, E., et al. 2024a, Astronomy & Astrophysics, 691, A145, doi: 10.1051/0004-6361/202347640
Maiolino, R., Scholtz, J., Witstok, J., et al. 2024b, Nature, 627, 59, doi: 10.1038/s41586-024-07052-5
Marconi, A., Risaliti, G., Gilli, R., et al. 2004, MNRAS, 351, 169, doi: 10.1111/j.1365-2966.2004.07765.x
Martins, F., Schaerer, D., & Marques-Chaves, R. 2026, arXiv e-prints, arXiv:2605.12141, doi: 10.48550/arXiv.2605.12141
Matthee, J., Naidu, R. P., Brammer, G., et al. 2024, ApJ, 963, 129, doi: 10.3847/1538-4357/ad2345
Morishita, T., Stiavelli, M., Mason, C. A., et al. 2026, ApJ, 998, 175, doi: 10.3847/1538-4357/ae3a7c
Morishita, T., Mason, C. A., Kreilgaard, K. C., et al. 2025, ApJ, 983, 152, doi: 10.3847/1538-4357/adbbdc
Mortlock, D. J., Warren, S. J., Venemans, B. P., et al. 2011, Nature, 474, 616, doi: 10.1038/nature10159
Muzzin, A., Suess, K. A., Marchesini, D., et al. 2025, arXiv e-prints, arXiv:2507.19706, doi: 10.48550/arXiv.2507.19706
Naidu, R. P., Matthee, J., de Graaff, A., et al. 2026a, arXiv e-prints, arXiv:2606.30711, doi: 10.48550/arXiv.2606.30711
Naidu, R. P., Matthee, J., Katz, H., et al. 2026b, Nature, 656, 329, doi: 10.1038/s41586-026-10846-4
Naidu, R. P., Oesch, P. A., Brammer, G., et al. 2026c, The Open Journal of Astrophysics, 9, 56033, doi: 10.33232/001c.156033
Nandal, D., & Loeb, A. 2026, ApJ, 998, 124, doi: 10.3847/1538-4357/ae32f3
Nandal, D., Whalen, D. J., Latif, M. A., & Heger, A. 2025, ApJL, 994, L11, doi: 10.3847/2041-8213/ae1a63
Napolitano, L., Castellano, M., Pentericci, L., et al. 2025, ApJ, 989, 75, doi: 10.3847/1538-4357/ade706
Newville, M., Stensitzki, T., Allen, D. B., & Ingargiola, A. 2014, LMFIT: Non-Linear Least-Square Minimization and Curve-Fitting for Python, 0.8.0 Zenodo, doi: 10.5281/zenodo.11813
Noboriguchi, A., Inoue, A. K., Nagao, T., Toba, Y., & Misawa, T. 2023, ApJL, 959, L14, doi: 10.3847/2041-8213/ad0e00
Oesch, P. A., Brammer, G., van Dokkum, P. G., et al. 2016, ApJ, 819, 129, doi: 10.3847/0004-637X/819/2/129
Oke, J. B., & Gunn, J. E. 1983, ApJ, 266, 713, doi: 10.1086/160817
Onoue, M., Kashikawa, N., Matsuoka, Y., et al. 2019, ApJ, 880, 77, doi: 10.3847/1538-4357/ab29e9
Onoue, M., Inayoshi, K., Ding, X., et al. 2023, ApJL, 942, L17, doi: 10.3847/2041-8213/aca9d3
Onoue, M., Silverman, J. D., Matsuoka, Y., et al. 2026, arXiv e-prints, arXiv:2609.09266, doi: 10.48550/arXiv.2609.09266
Pérez-González, P. G., Barro, G., Rieke, G. H., et al. 2024, ApJ, 968, 4, doi: 10.3847/1538-4357/ad38bb
Pollock, C. L., Gottumukkala, R., Heintz, K. E., et al. 2026, A&A, 708, A203, doi: 10.1051/0004-6361/202556032
Rantala, A. 2026, arXiv e-prints, arXiv:2604.22924, doi: 10.48550/arXiv.2604.22924
Richards, G. T., Lacy, M., Storrie-Lombardi, L. J., et al. 2006, The Astrophysical Journal Supplement Series, 166, 470, doi: 10.1086/506525
Rieke, G. H., Wright, G. S., Böker, T., et al. 2015, PASP, 127, 584, doi: 10.1086/682252
Rigby, J., Perrin, M., McElwain, M., et al. 2023, PASP, 135, 048001, doi: 10.1088/1538-3873/acb293
Rinaldi, P., Bonaventura, N., Rieke, G. H., et al. 2025, ApJ, 992, 71, doi: 10.3847/1538-4357/adfa10
Schwarz, G. 1978, Annals of Statistics, 6, 461
Shen, Y., Hall, P. B., Horne, K., et al. 2019, ApJS, 241, 34, doi: 10.3847/1538-4365/ab074f
Storey, P. J., & Zeippen, C. J. 2000, MNRAS, 312, 813, doi: 10.1046/j.1365-8711.2000.03184.x
Sun, W. Q., Naidu, R. P., Liu, H., et al. 2026, arXiv e-prints, arXiv:2609.09274, doi: 10.48550/arXiv.2609.09274
Tanaka, T. S., Akins, H. B., Harikane, Y., et al. 2025, ApJ, 995, 21, doi: 10.3847/1538-4357/ae145f
Taylor, A. J., Kokorev, V., Kocevski, D. D., et al. 2025, The Astrophysical Journal Letters, 989, L7, doi: 10.3847/2041-8213/ade789
Thomas, D., Steele, O., Maraston, C., et al. 2013, MNRAS, 431, 1383, doi: 10.1093/mnras/stt261

Torralba, A., Matthee, J., Weibel, A., et al. 2026a, ApJL, 1005, L37, doi: 10.3847/2041-8213/ae7bfd

Torralba, A., Matthee, J., Pezzulli, G., et al. 2026b, A&A, 707, A75, doi: 10.1051/0004-6361/202557537

Tripodi, R., D'Eugenio, F., Maiolino, R., et al. 2024, A&A, 692, A184, doi: 10.1051/0004-6361/202449980

Tripodi, R., Martis, N., Markov, V., et al. 2025, Nature Communications, 16, 9830, doi: 10.1038/s41467-025-65070-x

Trussler, J. A. A., Adams, N. J., Conselice, C. J., et al. 2023, MNRAS, 523, 3423, doi: 10.1093/mnras/stad1629

Übler, H., Maiolino, R., Pérez-González, P. G., et al. 2024, MNRAS, 531, 355, doi: 10.1093/mnras/stae943

Valentino, F., Brammer, G., Gould, K. M. L., et al. 2023, The Astrophysical Journal, 947, 20, doi: 10.3847/1538-4357/acbefa

Valentino, F., Heintz, K. E., Brammer, G., et al. 2025, A&A, 699, A358, doi: 10.1051/0004-6361/202553908

Virtanen, P., Gommers, R., Oliphant, T. E., et al. 2020, Nature Methods, 17, 261, doi: 10.1038/s41592-019-0686-2

Wang, F., Yang, J., Fan, X., et al. 2021, ApJL, 907, L1, doi: 10.3847/2041-8213/abd8c6

Williams, C. E., Naoz, S., Rose, S. C., et al. 2026, arXiv e-prints, arXiv:2603.26872, doi: 10.48550/arXiv.2603.26872

Willott, C. J., Albert, L., Arzoumanian, D., et al. 2010, AJ, 140, 546, doi: 10.1088/0004-6256/140/2/546

Yanagisawa, H., Ouchi, M., Kiyota, T., et al. 2026, arXiv e-prints, arXiv:2606.09726, doi: 10.48550/arXiv.2606.09726

Yang, D., Hennawi, J. F., Guarneri, F., et al. 2026, A&A, 711, A104, doi: 10.1051/0004-6361/202658883

Yang, J., Wang, F., Fan, X., et al. 2020, ApJL, 897, L14, doi: 10.3847/2041-8213/ab9c26

Yu, Q., & Tremaine, S. 2002, MNRAS, 335, 965, doi: 10.1046/j.1365-8711.2002.05532.x

Zou, F., Gallo, E., Zuo, Z., et al. 2026, arXiv e-prints, arXiv:2603.24893, doi: 10.48550/arXiv.2603.24893

Zwick, L., Tiede, C., & Mayer, L. 2026, ApJ, 1002, 7, doi: 10.3847/1538-4357/ae4d47